Pol. J. Environ. Stud. Vol. XX, No. X (XXXX), 1-20

DOI: *10.15244/pjoes/224841* ONLINE PUBLICATION DATE: 2026-08-10

Original Research

Long-Term Differentiation and Associated Drivers of Ecological Resilience in Ecologically Livable Villages: Evidence from the Yangtze River Delta, China

Ziqiang Zhang[1], Xianhua Sun[1]*, Sucheng Yao[2]

[1]College of Art and Design, Nanjing Forestry University, Nanjing 210000, China
[2]Faculty of Landscape Engineering, Suzhou Polytechnic Institute of Agriculture, Suzhou 215000, China

Received: 23 April 2026
Accepted: 19 June 2026

Abstract

Long-term differentiation in ecological resilience within ecologically livable villages remains insufficiently understood under rapid urbanization and persistent land-use change. Using a regional-scale sample of 1,090 ecologically livable villages in the Yangtze River Delta, this study constructed an ecological resilience index (ERI) and its three dimensions – resistance, adaptability, and recovery – and identified spatial patterns and temporal trends in 2003, 2008, 2013, 2018, and 2023. The 1,090-village sample was used as the main regional-scale sample to identify long-term ERI patterns and regional background explanatory variables, whereas the 107-village corridor sample was introduced as a supplementary mechanism sample to examine local spatial configuration factors under a relatively similar Yangtze corridor context. We then applied XGBoost-SHAP to characterize variable importance, SHAP contribution directions, and nonlinear response ranges in the regional-scale and corridor-level analyses. ERI remained broadly stable from 2003 to 2023, but spatial differentiation persisted. Runoff, cropland proportion, and precipitation were the dominant explanatory variables associated with ERI in 2023. In the corridor sample, road density, POI density, and road length showed higher explanatory power than other local mechanism variables. These findings show that persistent differentiation was jointly associated with long-term regional patterns, regional background conditions, and local environmental and spatial configuration factors, and they provide an empirical basis for environmental assessment, spatial configuration optimization, and differentiated management in ecologically livable villages.

Keywords: ecological resilience, ecologically livable villages, Yangtze River Delta, XGBoost-SHAP, environmental management

*e-mail: sun.xianhua@163.com
0009-0006-0905-6344

Introduction

Under rapid urbanization and continuing land-use change, rural areas have become important spaces shaped by environmental change, ecological pressure, and human activities [1, 2]. The Yangtze River Delta is a highly integrated region in China, characterized by intensive factor mobility and persistent land-use transition. Its rural ecological conditions and long-term changes, therefore, provide an important case for environmental research [3]. Ecological resilience reflects the capacity of rural ecosystems to maintain basic functions, adjust, and recover after disturbance. It also helps explain why villages within the same region may show different ecological conditions [4-6]. This issue is particularly important for ecologically livable villages (EL villages). Although EL villages are usually regarded as having a relatively good ecological foundation, this does not mean that their internal ecological conditions are homogeneous [7, 8]. Even under similar policy orientations, villages may still show persistent differentiation in ecological resilience. A key question, therefore, remains: why does ecological resilience continue to differentiate within EL villages, and how is this differentiation associated with regional and local conditions?

Existing research still has three major limitations in addressing this question. First, many studies rely on single-year or short-term data, which makes it difficult to identify long-term patterns and their stability at the village scale [9-12]. Second, analyses of explanatory factors often remain at the level of linear relationships or average associations, with limited attention to nonlinear responses and possible sensitive ranges. Third, evidence on local mechanisms remains insufficient, especially for identifying local environmental and spatial configuration factors that can further distinguish current differences under similar regional backgrounds. As a result, existing studies can describe overall change and identify some key variables, but they still cannot adequately explain why ecological resilience continues to differentiate within EL villages. Addressing this question requires a unified framework that links long-term patterns, key background explanatory variables, and supplementary evidence on local mechanisms.

Assessing and explaining rural ecological resilience requires attention to long-term change, spatial variation, and possible nonlinear relationships [13-15]. Traditional methods, such as regression and fixed-effects models, are mainly based on linear assumptions. They are often limited when dealing with high-dimensional variables and complex interactions. This limitation is especially evident in village-scale studies with multiple data sources, where such methods tend to remain at the level of overall average associations and have difficulty identifying association directions and sensitive ranges of key variables. At the same time, multi-source data supported by remote sensing and GIS provide a stable basis for long-term monitoring and improve the comparability of indicators across regions [16]. This makes it possible to construct an ecological resilience index (ERI) and its component dimensions over a relatively long period. On this basis, interpretable machine-learning methods such as XGBoost can capture nonlinear relationships and variable interactions under high-dimensional conditions. Combined with SHAP, they can further identify variable importance, SHAP contribution directions, and nonlinear response ranges, thereby improving interpretability and testability.

Against this background, this study focuses on EL villages in the Yangtze River Delta and adopts a two-stage research design. In the first stage, the regional-scale main sample of 1,090 EL villages was used to construct the ERI and its three dimensions, namely resistance (RES), adaptability (ADP), and recovery (REC). The spatial patterns and temporal trends of these indicators were then identified in 2003, 2008, 2013, 2018, and 2023. Based on these results, the background explanatory variables associated with ERI in 2023 were further identified, and the XGBoost-SHAP framework was used to examine variable importance, SHAP contribution patterns, and nonlinear response ranges. In the second stage, a supplementary sample of 107 villages in the Yangtze corridor was introduced to examine local mechanisms. The corridor sample was introduced because regional-scale natural and climatic variables alone cannot fully capture local spatial configuration conditions, such as road accessibility, POI agglomeration, and service distribution. Therefore, the corridor analysis provides supplementary evidence rather than a separate or competing analysis. Roads, POIs, service accessibility, and blue-green variables were introduced to identify local environmental and spatial configuration factors that could further explain current differences within the sensitive zone of the Yangtze corridor. The ERI and its three dimensions in both samples were calculated using the same indicator system and weighting method, which ensured consistent measurement. Differences in explanatory variables reflected different analytical tasks rather than missing data. The main sample of 1,090 EL villages was used to identify long-term patterns and regional-scale background explanatory variables, whereas the corridor sample was used to examine supplementary local mechanism evidence under corridor conditions.

This study makes three main contributions to the understanding of persistent differentiation in EL villages. First, it identifies persistent differentiation under long-term patterns within the same group of EL villages, which helps avoid judging ecological conditions only from overall average change. Second, it links regional-scale background explanatory variables with supplementary local mechanism evidence from the Yangtze corridor, which helps explain internal differences across spatial levels. Third, under a unified ecological resilience indicator system, it jointly examines long-term patterns, key background explanatory variables, and local environmental and spatial configuration factors. This provides a clearer basis for environmental assessment, spatial configuration optimization, and differentiated management in EL villages.

Accordingly, this study addresses three research questions:

(1) What spatial patterns and trend distributions did the ERI of the 1,090 EL villages show from 2003 to 2023 when constructed from the three dimensions of RES, ADP, and REC?

(2) Which natural and climatic explanatory variables were most strongly associated with ERI in 2023, and what were their SHAP contribution directions and nonlinear response ranges?

(3) In the corridor sample, which local environmental and spatial configuration factors could further explain current differences in ERI, and did they differ in importance and response range?

Materials and Methods

Study Area and Samples

The study area was the Yangtze River Delta. This region had a high level of urbanization, active land-use change, and concentrated rural transformation. It was therefore well-suited for village-scale analysis of ecological resilience.

This study adopted a two-stage sample design. In the first stage, the regional-scale main sample of 1,090 ecologically livable villages (EL villages) was used to identify the spatial patterns, trend distribution, and key natural and climatic explanatory variables associated with ecological resilience from 2003 to 2023. In the second stage, a supplementary sample of 107 villages in the Yangtze corridor for local mechanism analysis (hereafter, the corridor sample) was used to identify which local environmental and spatial configuration factors could further explain current differences in ecological resilience within the sensitive zone of the Yangtze corridor. ERI and its three dimensions were calculated for both samples using the same ecological resilience indicator system and weighting scheme to ensure consistent measurement.

The sample of 1,090 EL villages was compiled from nationally released village lists with an ecological-livability orientation, including National Forest Villages, China's Most Attractive Leisure Villages, China's Beautiful Leisure Villages, Top 100 Beautiful Villages in China, and Model Beautiful and Livable Villages. These records were standardized, deduplicated, and spatially matched to generate the final sample. The sample of 107 villages in the Yangtze corridor was obtained by delineating a 20-km corridor along both sides of the Yangtze River mainstem and then screening villages based on village locations within this corridor.

The corridor sample was used to provide additional evidence on how local environmental and spatial configuration differences were associated with the current ecological resilience pattern. It was not intended to replace the regional-scale main sample of 1,090 EL villages. Overall, the 1,090 EL villages covered the major rural areas of the Yangtze River Delta, whereas the corridor sample was mainly distributed along the Yangtze River mainstem and its adjacent belt-like areas. Fig. 1 shows the study area, the spatial distribution of the 1,090 EL villages, and the 2-km buffers of the 107 corridor villages.

Rationale for the Two-Stage Sample Design

The two samples were designed for different analytical purposes. The 1,090 EL villages constituted the main regional-scale sample and were used to identify long-term ERI differentiation and regional background explanatory variables. The 107 corridor villages were not intended to replace the regional sample or to generalize the mechanism results to all EL villages in the Yangtze River Delta. Instead, they were introduced as a supplementary mechanism sample to examine whether local spatial configuration variables, including road density, POI density, service accessibility, and blue-green spatial conditions, could further distinguish current ERI differences under the Yangtze corridor context. This design allowed the study to link regional-scale long-term differentiation with additional local mechanism evidence while maintaining a consistent ERI measurement framework across the two samples.

Overall Analytical Framework

Based on the sample design described above, this study developed an overall analytical framework consisting of long-term pattern identification, background explanatory-variable analysis, and local mechanism analysis (Fig. 2).

The first part used the regional-scale main sample of 1,090 ecologically livable villages (EL villages) to construct the ecological resilience index (ERI) and to identify the spatial patterns and trend distribution of ecological resilience in 2003, 2008, 2013, 2018, and 2023.

The second part used ERI in 2023 as the target variable and applied the XGBoost-SHAP framework to identify key natural and climatic explanatory variables associated with ERI. It further examined their importance, SHAP contribution directions, and nonlinear response characteristics to describe the regional-scale background explanatory structure.

The third part used the corridor sample for local mechanism analysis. Roads, POIs, service accessibility, and blue-green variables were introduced to identify local environmental and spatial configuration factors that could further explain current differences in ecological resilience under similar regional backgrounds.

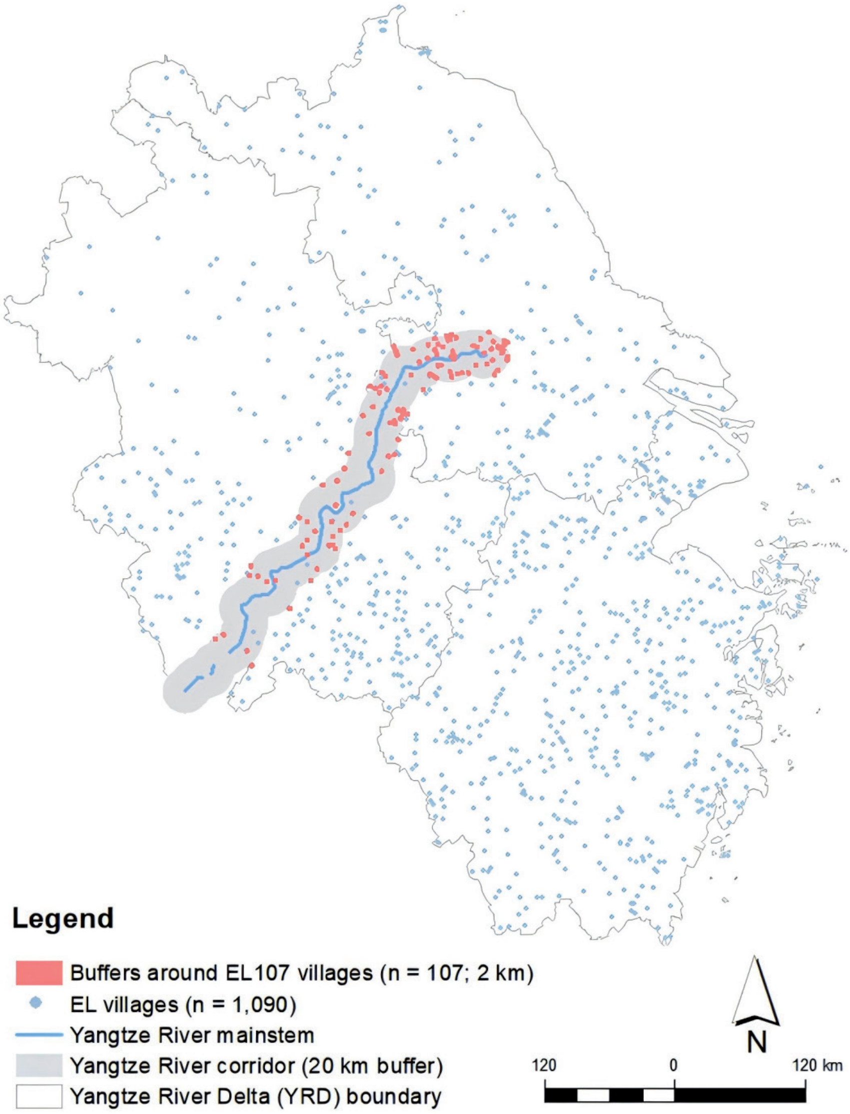

Fig. 1. Study area, spatial distribution of the 1,090 ecologically livable villages, and the 107 villages in the corridor sample with 2-km buffers.

Variable Definition and Data Sources

This study used two groups of variables. One group was used for the analysis of regional-scale background explanatory variables based on the regional-scale main sample of 1,090 ecologically livable villages (EL villages). The other group was used for local mechanism analysis based on the corridor sample. Variable definitions are presented in Table 1, and data sources are listed in Table 2.

For the regional-scale analysis, the outcome variables included the ecological resilience index (ERI), resistance (RES), adaptability (ADP), recovery (REC), and the Theil-Sen slope of ERI during 2003–2023 (ERI_sen). ERI and its three dimensions were used to represent village-scale ecological resilience, whereas ERI_sen was used to indicate the direction and intensity of long-term change. The core explanatory variables in the 2023 regional background model included cropland_pct, pct_impervious, ro_mean, pr_mean, tmmx_mean, srad_mean, and nl_mean. These variables represented land-use structure, impervious surface conditions, hydrological conditions, climatic conditions, and human activity intensity, respectively.

For the corridor sample, the outcome variables remained consistent with those in the regional-scale analysis and included ERI and its three dimensions. In addition, this sample incorporated road-network data, POI data, population grids, and blue-green variables for local mechanism analysis.

Data preprocessing included four steps. First, all datasets were standardized to the same coordinate system and spatial extent. Second, continuous raster data were extracted to the village scale to generate mean values, proportions, or density indicators. Third, road length, road density, POI counts, and facility density were calculated by combining village boundaries with 2-km buffers. Fourth, field names were standardized,

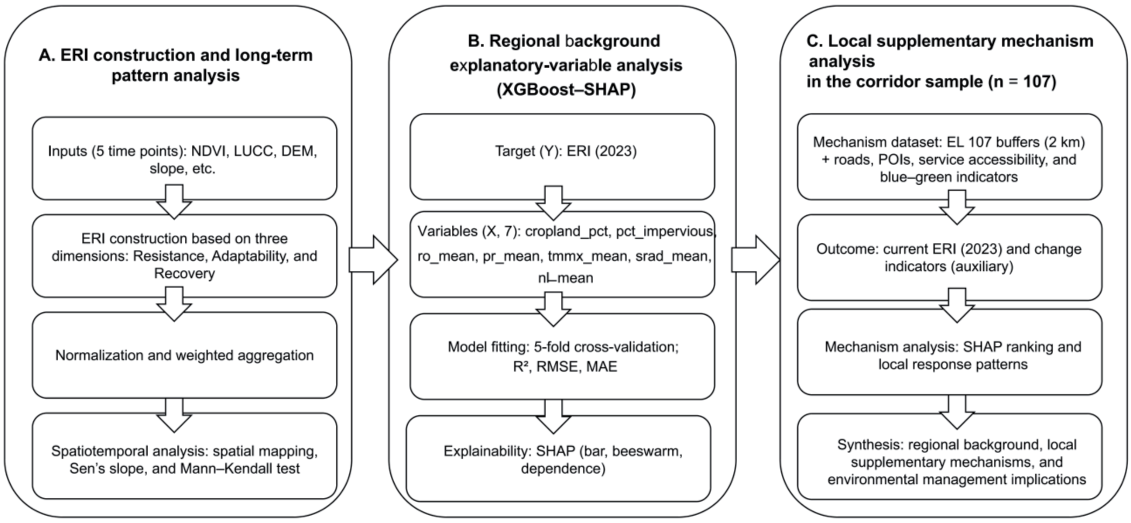

Fig. 2. Overall analytical framework: long-term pattern identification, background explanatory-variable analysis, and local mechanism analysis.

and missing values and duplicate records were checked to generate a village-scale database for trend analysis, background explanatory-variable identification, and local mechanism analysis.

The regional-scale main sample of 1,090 EL villages was used to identify regional-scale background explanatory variables, whereas the corridor sample was used to examine local mechanisms under corridor conditions. The local environmental and spatial configuration variables in the corridor sample were used only to explain current differences in ERI.

Table 1. Variable definitions used in this study (EL villages).

Panel A. Regional-scale variables for the full EL sample (n = 1,090)					
Group	Variable	Symbol / column	Definition	Unit	Spatial scale/ Year(s)
Outcome (Y)	Ecological resilience index (ERI)	eri_2003, eri_2008, eri_2013, eri_2018, eri_2023	Composite ERI based on RES / ADP / REC	dimensionless (0–1)	Village unit / 2003, 2008, 2013, 2018, 2023
	RES / ADP / REC	res_2023; adp_2023; rec_2023	Three dimensions of ERI in 2023	dimensionless (0–1)	Village unit / 2023
	ERI trend (Sen slope)	eri_sen_03_23	Theil–Sen slope of ERI during 2003–2023	index per year	Village unit / 2003–2023
Explanatory variable (X)	Cropland proportion	cropland_pct	Share of cropland within the village unit	0–1 proportion	Village unit / 2023
	Impervious surface proportion	pct_impervious	Share of impervious surface within the village unit	0–1 proportion	Village unit / 2023
	Mean runoff	ro_mean	Mean runoff condition	raster original unit	Village unit / 2023
	Annual precipitation	pr_mean	Mean annual precipitation	mm	Village unit / 2023
	Maximum temperature	tmmx_mean	Mean maximum temperature	ºC	Village unit / 2023
	Solar radiation	srad_mean	Mean solar radiation	raster original unit	Village unit / 2023
	Nighttime light	nl_mean	Mean nighttime light as a proxy for human activity	raster original unit	Village unit / 2023

Table 1 (continued)

Panel B. Local supplementary mechanism variables for corridor villages (n = 107)					
Group	Variable	Symbol / column	Definition	Unit	Spatial scale/ Year(s)
Outcome (Y)	Current ecological resilience index	23eri	Current ERI of corridor villages	dimensionless (0–1)	Village unit / 2023
	Change in ERI (auxiliary)	dERI_03_23	Change in ERI between 2003 and 2023	dimensionless	Village unit / 2003–2023
Mechanism (X)	Road density	road_den_ kmkm²	Road length per area within the 2-km buffer	km/km²	2-km buffer / 2023
	POI density	poi_den	Density of all POIs within the 2-km buffer	count/km²	2-km buffer / 2023
	Road length within 2-km buffer	road_len_m_2k	Total road length within the 2-km buffer	m	2-km buffer / 2023
	Basic-service POI count	poi_cnt_2k	Count of education, medical, eldercare, and transport POIs within the 2-km buffer	count	2-km buffer / 2023
	Basic-service POI density	p01_den	Density of basic-service POIs within the 2-km buffer	count/km²	2-km buffer / 2023
	Cultural POI density	cul_den	Density of cultural POIs within the 2-km buffer	count/km²	2-km buffer / 2023

Table 2. Datasets used in this study, including format, spatial resolution, time coverage, source, and analytical role.

Data	Format	Spatial resolution	Time coverage	Source	Analytical role
EL villages and corridor subset	SHP	Village unit	2003–2023 / 2023	Authors' compilation	Analysis units; corridor subset and 2-km buffers
Yangtze River mainstem and corridor	SHP	Vector	Static	OSM / official hydrography	Corridor delineation and subset selection
OSM road network	SHP	Vector	latest available snapshot	Geofabrik (OSM)	Proxy for current road configuration, road length, density, and accessibility
OSM POIs	SHP	Vector	latest available snapshot	Geofabrik (OSM)	Proxy for current service accessibility and local facility agglomeration
Population grid (GHS-POP)	GeoTIFF	100–250 m	2020	JRC GHSL	Population proxy for local mechanism analysis
MODIS NDVI (annual aggregates)	GeoTIFF	500 m	2003 / 2008 / 2013 / 2018 / 2023	NASA LP DAAC (AppEEARS)	NDVI mean within 2-km buffers
MODIS land cover	GeoTIFF	500 m	2003 / 2008 / 2013 / 2018 / 2023	NASA LP DAAC (AppEEARS)	Water reclassification and water proportion
CLCD land cover	GeoTIFF	30 m	2003 and 2023	CLCD provider	Green/water share and landscape metrics
DEM + slope	GeoTIFF	30 m	Static	Public DEM	Elevation and slope extraction
ES/HQ rasters (WY, SC, CS, HQ)	GeoTIFF	30 m	2003 and 2023	Provided / InVEST outputs	Resistance indicators and zonal mean extraction
Derived indices (authors' calculations)	CSV	Village unit	2003–2023	Authors' calculations	RES, ADP, REC, ERI, and ERI_sen

Notes: ERI = ecological resilience index; RES/ADP/REC = resistance/adaptability/recovery; OSM = OpenStreetMap; GHSL = Global Human Settlement Layer; NDVI = normalized difference vegetation index; CLCD = China Land Cover Dataset. For corridor-level local mechanism analysis, the latest available road, POI, and population datasets were used as proxies for current local spatial configuration, service accessibility, and population conditions. These variables were introduced only for the cross-sectional interpretation of current local differences rather than for historical reconstruction.

Construction of the Ecological Resilience Index

This study constructed the ecological resilience index (ERI) at the village scale and represented it using three dimensions: resistance (RES), adaptability (ADP), and recovery (REC). The indicator composition, direction, and weights are shown in Table 3.

Rationale for Indicator Selection and Weighting Strategy

Ecological resilience was represented by resistance, adaptability, and recovery because these three dimensions jointly describe the ability of rural ecosystems to maintain ecological functions, adjust to disturbance, and recover ecological conditions. Resistance reflects the capacity of a rural ecosystem to maintain basic ecological services and habitat conditions when facing external disturbance. Adaptability reflects the structural and environmental conditions that support adjustment under changing land-use and environmental contexts. Recovery reflects the potential of vegetation, green space, and water-related ecological elements to regenerate or restore ecological conditions after disturbance. Therefore, the RES–ADP–REC framework provides a functional basis for constructing the village-scale ERI.

The specific indicators were selected according to their ecological meanings and their relevance to the three dimensions of resilience. In the RES dimension, water yield, sediment retention or soil conservation, carbon storage, and habitat quality were used to represent the capacity of rural ecosystems to maintain hydrological regulation, soil conservation, carbon retention, and habitat conditions. In the ADP dimension, the Shannon diversity index, Shannon evenness index, largest patch index, elevation, and slope were used to represent landscape structure, spatial heterogeneity, patch dominance, and topographic constraints that may affect ecological adjustment. In the REC dimension, NDVI, green coverage ratio, and surface water ratio were used to represent vegetation recovery, green-space support, and water-related ecological support. These indicators, therefore, link the conceptual dimensions of ecological resilience with observable village-scale ecological and spatial conditions.

Equal weighting was adopted to maintain transparency and comparability across years and samples. This strategy does not assume that all indicators have identical ecological effects in reality. Instead, it avoids introducing additional subjective weights in the absence of a widely accepted weighting standard for ERI construction in EL villages. At the dimension level, RES, ADP, and REC were treated as conceptually complementary components of ecological resilience, and each dimension was therefore assigned one-third of the final ERI. Within each dimension, equal weights were used to keep the calculation procedure consistent and reproducible across the regional-scale sample and the corridor sample.

For habitat-quality-related indicators, the determination of indicator direction and parameter settings followed relevant studies on the InVEST habitat quality module [17]. All indicators were extracted to the village scale and prepared for the corresponding years in both the regional-scale main sample of 1,090 ecologically livable villages (EL villages) and the corridor sample. The processing strategy for multi-temporal remote-sensing indicators related to ecological quality followed relevant studies on remote-sensing ecological indices [18].

Table 3. Ecological resilience index (ERI) construction, indicator direction, and weighting scheme.

Dimension	Indicator	Symbol	Direction	Standardization	Weight
Resistance (RES)	Water yield	wy_mean	+	min–max (x − min)/(max − min)	0.25
	Sediment retention / soil conservation	sr_mean	+	min–max (x − min)/(max − min)	0.25
	Carbon storage	cs_mean	+	min–max (x − min)/(max − min)	0.25
	Habitat quality / degradation	hq_mean	+/(−)*	see note*	0.25
Adaptability (ADP)	Shannon diversity index	shdi	+	min–max (x − min)/(max − min)	0.20
	Shannon evenness index	shei	+	min–max (x − min)/(max − min)	0.20
	Largest patch index	lpi	+	min–max (x − min)/(max − min)	0.20
	Elevation (DEM)	elev_mean	−	reverse min–max (max − x)/(max − min)	0.20
	Slope	slope_mean	−	reverse min–max (max − x)/(max − min)	0.20
Recovery (REC)	NDVI (annual max)	ndvi	+	min–max (x − min)/(max − min)	0.333
	Green coverage ratio	green_pct	+	min–max (x − min)/(max − min)	0.333
	Surface water ratio	water_pct	+	min–max (x − min)/(max − min)	0.333

Note: If habitat quality is used, it is treated as a positive indicator; if habitat degradation is used, reverse standardization is applied.

To ensure comparability among indicators, all original variables were standardized. Positive indicators were normalized using min-max standardization, as shown in Eq. (1), whereas negative indicators were standardized using reverse min-max normalization, as shown in Eq. (2). In this study, elevation and slope were treated as negative indicators. For habitat-quality-related indicators, the direction depended on the data layer used. Habitat quality values were treated as positive indicators, whereas habitat degradation values were treated as negative indicators.

$$Z_i j = (x_i j - x_j, \min)/(x_j, \max - x_j, \min) \tag{1}$$

$$Z_i j = (x_j, \max - x_i j)/(x_j, \max - x_j, \min) \tag{2}$$

where $Z_i j$ denotes the standardized value of indicator j for village i, $x_i j$ is the original value, and x_j,min and x_j,max are the minimum and maximum values of indicator j in the sample, respectively.

After standardization, the indicators were aggregated within each dimension using weighted sums. RES included four indicators, each with a weight of 0.25. ADP included five indicators, each with a weight of 0.20. REC included three indicators, each with a weight of 0.333. The three dimensions were calculated using Eqs. (3)-(5), respectively.

$$RES_i = \Sigma(j = 1 \rightarrow 4) w_j Z_i j \tag{3}$$

$$ADP_i = \Sigma(j = 1 \rightarrow 5) w_j Z_i j \tag{4}$$

$$REC_i = \Sigma(j = 1 \rightarrow 3) w_j Z_i j \tag{5}$$

where w_j is the weight of indicator j, and $Z_i j$ is the standardized indicator value. The final ERI was then obtained by assigning equal weights to the three dimensions, as shown in Eq. (6).

$$ERI_i = (\frac{1}{3}) RES_i + (\frac{1}{3}) ADP_i + (\frac{1}{3}) REC_i \tag{6}$$

where ERI_i denotes the composite ecological resilience index of village i, and RES_i, ADP_i and REC_i denote the composite scores of resistance, adaptability, and recovery for village i, respectively.

Trend Analysis

Trend analysis was conducted for the ecological resilience index (ERI) of the 1,090 ecologically livable villages (EL villages) at five time points: 2003, 2008, 2013, 2018, and 2023. The Theil-Sen slope estimator was used to quantify the overall magnitude of change [19], and the Mann-Kendall test was used to evaluate trend significance [20, 21]. The Theil-Sen slope is given in Eq. (7).

$$\beta = \text{Median}\left(\frac{x_j - x_i}{t_j - t_i}\right), j > i \tag{7}$$

where β denotes the trend slope, x_i and x_j are the ERI values at time points i and j, and t_i and t_j are the corresponding years.

The Mann-Kendall test first calculates the statistic S, as shown in Eq. (8), where n is the length of the time series and $\text{sgn}(x_j - x_k)$ is the sign function defined in Eq. (9). The statistic is then standardized to Z, as shown in Eq. (10), to determine trend direction and significance. When Z>0, the time series shows an increasing trend. When Z<0, it shows a decreasing trend. When Z = 0, no clear trend is indicated. Statistical significance is further determined by comparing Z with the critical value at a given significance level.

$$S = \sum_{k=1}^{n-1} \sum_{j=k+1}^{n} \text{sgn}\,(x_j - x_k) \tag{8}$$

$$\begin{aligned} \text{sgn}(x_j - x_k) &= 1, \quad \text{if}\, x_j - x_k > 0 \\ \text{sgn}(x_j - x_k) &= 0, \quad \text{if}\, x_j - x_k = 0 \\ \text{sgn}(x_j - x_k) &= -1, \text{if} x_j - x_k < 0 \end{aligned} \tag{9}$$

$$\begin{aligned} Z &= \frac{(S-1)}{\sqrt{\text{Var}(S)}}, \quad \text{if}\, S > 0\ Z = 0, \\ \text{if}\, S = 0 Z &= \frac{(S+1)}{\sqrt{\text{Var}(S)}}, \quad \text{if}\, S < 0 \end{aligned} \tag{10}$$

XGBoost-SHAP-based Identification of Explanatory Variables

This study used XGBoost to model the statistical associations between ERI and explanatory variables, and applied SHAP to interpret variable importance, SHAP contribution direction, and local response characteristics [22, 23]. In this study, the identified variables are interpreted as model-based explanatory variables associated with ERI variation, rather than as confirmed causal factors.

A total of four models were constructed to address four analytical tasks. Model-1 used ERI in 2023 as the target variable to identify key natural and climatic explanatory variables associated with current ecological resilience. Model-2 used the Theil-Sen slope of ERI during 2003-2023 as the target variable to identify explanatory variables associated with long-term change. Model-3 used ERI in 2023 in the corridor sample to examine the explanatory role of local mechanism variables in current differences in ecological resilience. Model-4 used the change in ERI in the same corridor sample as the target variable to examine the supplementary explanatory role of mechanism variables

Table 4. Summary of model settings and performance

Model	Target variable / task	Sample size	No. of features	Validation strategy	R^2 (mean)	RMSE (mean)	MAE (mean)	Key hyperparameters
Model-1	2023 ERI (regional)	1090	7	5-fold cross-validation	0.873	0.058	0.022	n_estimators = 500, max_depth = 4, learning_rate = 0.05
Model-2	ERI_sen, 2003–2023	1090	7	5-fold cross-validation	0.573	0.036	0.001	n_estimators = 500, max_depth = 4, learning_rate = 0.05
Model-3	2023 ERI (corridor)	107	6	5-fold cross-validation	0.909	0.080	0.005	n_estimators = 500, max_depth = 4, learning_rate = 0.05
Model-4	ΔERI, 2003–2023	107	6	5-fold cross-validation	0.437	0.058	0.023	n_estimators = 500, max_depth = 4, learning_rate = 0.05

Note: ERI = ecological resilience index; ERI_sen = Theil–Sen slope of ERI during 2003–2023; ΔERI = change in ERI between 2003 and 2023; RMSE = root mean square error; MAE = mean absolute error.

in the change process. The sample size, number of features, validation strategy, evaluation metrics, and key hyperparameters of the four models are reported in Table 4.

For regional-scale background explanatory-variable identification, the analysis was based on the regional-scale main sample of 1,090 ecologically livable villages (EL villages). The explanatory variables included cropland_pct, pct_impervious, ro_mean, pr_mean, tmmx_mean, srad_mean, and nl_mean. The response variables were ERI in 2023 and ERI_sen, respectively. Model performance was evaluated using five-fold cross-validation and three metrics: R-squared, RMSE, and MAE. The coefficient of determination R^2 is given in Eq. (11).

$$R^2 = 1 - \frac{\sum_{i=1}^{n}(y_i - \hat{y}_i)^2}{\sum_{i=1}^{n}(y_i - \bar{y})^2} \tag{11}$$

where y_i denotes the observed value, $\hat{y}_i$ denotes the predicted value, $\bar{y}_i$ is the mean of the observed values, and n is the sample size. R^2 measures the proportion of variance in the target variable explained by the model.

The root mean square error RMSE is calculated as follows:

$$RMSE = \sqrt{\frac{1}{n}\sum_{i=1}^{n}(y_i - \hat{y}_i)^2} \tag{12}$$

where y_i denotes the observed value, $\hat{y}_i$ denotes the predicted value, and n is the sample size. RMSE measures the overall magnitude of prediction error.

The mean absolute error MAE is calculated as follows:

$$MAE = \frac{1}{n}\sum_{i=1}^{n}|y_i - \hat{y}_i| \tag{13}$$

where y_i denotes the observed value, $\hat{y}_i$ denotes the predicted value, and n is the sample size. MAE measures the average deviation between predicted and observed values.

To interpret model outputs, this study further applied the SHAP method [23]. Its additive form is shown in Eq. (14).

$$f(x_i) = \phi_0 + \sum_{j=1}^{m}\phi_{ij} \tag{14}$$

where $f(x_i)$ denotes the predicted value for sample i, ϕ_0 is the baseline prediction of the model, ϕ_{ij} denotes the SHAP contribution of variable j to the prediction for sample i, and m is the number of variables.

Local Mechanism Analysis in the Yangtze Corridor

Local mechanism analysis was conducted using the corridor sample. These villages are located within a 20-km corridor along both sides of the Yangtze River mainstem, and a 2-km buffer was constructed around each village point. For descriptive statistics, the outcome variables remained consistent with those used in the regional-scale analysis, namely the ecological resilience index (ERI) and its three dimensions. Variable definitions are presented in Table 1, and data sources are listed in Table 2.

The mechanism variables included road density, POI density, road length within the 2-km buffer, basic-service POI count, basic-service POI density, and cultural POI density [24]. Road and POI variables were used to represent local spatial configuration and service accessibility [25]. Because time-consistent road and POI datasets at the village scale were not available for all target years, the latest available datasets were used as proxies for current local spatial configuration and service accessibility. Their length, count, and density were calculated using buffer-based statistics, and the extracted variables were then checked and standardized.

The two target variables in the mechanism models were ERI in 2023 and the change in ERI during 2003-2023. Model settings and performance metrics are reported in Table 4. During the initial screening stage, additional variables, including distance to the nearest town center, total population, a proxy for population density, mean NDVI, and water proportion, were also compared. However, only road variables, POI variables, and their related density and count indicators are reported in the main text.

Descriptive Statistics

The descriptive statistics are presented in Table 5. For the regional-scale main sample of 1,090 ecologically livable villages (EL villages), Table 5 reports ERI and its three dimensions in 2023, together with the regional-scale background explanatory variables. For these regional background explanatory variables, Table 5 reports descriptive statistics for the standardized variables used in the final models.

Results and Discussion

Spatial Patterns and Evolution of ERI during 2003-2023

The spatial distribution of ERI in 2003 and 2023 is shown in Fig. 3, and the temporal distribution and trend characteristics of ERI during 2003-2023 are shown in Fig. 4. Overall, the spatial pattern of ERI remained relatively stable during the study period. Higher ERI values were mainly concentrated in the southern part of the region, whereas the northern and northwestern areas were characterized by lower values. Villages in the Yangtze corridor and adjacent areas showed moderate to relatively high ERI values in both 2003 and 2023.

From a long-term perspective, changes in ERI were limited in most villages. Sen's slope values were concentrated around zero. Among the 1,090 villages, 1,035 were classified as having no clear trend, whereas only 47 and 8 villages showed increasing and decreasing trends, respectively. These results indicate that ERI in EL villages in the Yangtze River Delta did not exhibit a widespread significant increase or decrease during 2003-2023.

The spatial distribution of trends further shows that positive changes were more common in the eastern part of the region and in areas associated with the Yangtze corridor, whereas negative changes were more scattered and limited in number. Overall, ERI in EL villages in the Yangtze River Delta was characterized by persistent spatial differentiation under a broadly stable regional pattern during the study period.

Model Performance and Key Explanatory Variables Associated with ERI in 2023

The predictive performance of the four models is shown in Fig. 5. The four models correspond to different analytical tasks. Model-1 identifies the key explanatory variables associated with ERI in 2023. Model-2 examines the explanatory variables associated with ERI trends during 2003-2023. Model-3 examines the explanatory role of mechanism variables for ERI in 2023 in the corridor sample. Model-4 examines the mechanism variables associated with the change in ERI in the same corridor sample. Model performance differed across the four analytical tasks. The R^2 values of Model-1 and Model-3 were 0.873 and 0.909, respectively, whereas those of Model-2 and Model-4 were 0.573 and 0.437. Compared with current ERI levels, long-term trends and change processes showed lower explanatory power. The following results focus on the key explanatory variables identified by Model-1.

The SHAP summary results of Model-1 are shown in Fig. 6. The global importance ranking indicates that ro_mean had the highest mean absolute SHAP value and contributed more strongly than the other variables. cropland_pct and pr_mean ranked second and third, respectively. nl_mean followed, whereas pct_impervious, tmmx_mean, and srad_mean showed relatively lower contributions. Overall, differences in ERI in 2023 were mainly associated with a small number of high-contribution variables.

The beeswarm distribution further shows that the SHAP contribution directions and value ranges differed across variables. ro_mean displayed the clearest directional separation. High values were mainly concentrated in the positive SHAP range, whereas low values were mainly located in the negative SHAP range, and its overall distribution span was the widest. cropland_pct showed a clear two-sided pattern, with high values more often associated with negative contributions and low-to-moderate values more often associated with positive contributions. In contrast, pr_mean showed a relatively wide distribution on both sides of zero. Overall, Fig. 6 indicates that high-contribution variables differed not only in global importance but also in their local distribution ranges.

Nonlinear Response Ranges of Key Explanatory Variables Associated with ERI

The nonlinear response characteristics of the four key explanatory variables are shown in Fig. 7. All four variables displayed clear range differences in their SHAP contribution patterns and did not vary monotonically across their value ranges.

For ro_mean, SHAP values showed an overall increasing pattern. Its SHAP values gradually shifted from negative contributions in the low-value range to positive contributions in the high-value range, and the positive SHAP contribution further increased at higher

Table 5. Descriptive statistics of the main variables retained in the final main-text analysis.

Group	Variable	1090 N	1090 Mean	1090 SD	1090 P25	1090 Median	1090 P75	107 N	107 Mean	107 SD	107 P25	107 Median	107 P75
Outcomes (2023)	ERI (2023)	1090	0.3656	0.0806	0.293	0.3775	0.427	107	0.3895	0.2365	0.2317	0.2741	0.4728
	RES (2023)	1090	0.2912	0.126	0.1973	0.2875	0.383	107	0.2989	0.2388	0.1165	0.1893	0.4197
	ADP (2023)	1090	0.4306	0.1243	0.333	0.4335	0.524	107	0.5762	0.3732	0.3549	0.4214	0.6615
	REC (2023)	1090	0.4595	0.1473	0.321	0.471	0.6058	107	0.3609	0.0886	0.3055	0.3342	0.3874
Regional background explanatory variables (1090 only)	Cropland proportion	1090	-0.000193	0.004913	-0.001949	0.000177	0.001562	—	—	—	—	—	—
	Impervious surface proportion	1090	0.002042	0.003546	0.000155	0.000727	0.002328	—	—	—	—	—	—
	Mean runoff	1090	0.3211	0.3187	0.1255	0.3243	0.5408	—	—	—	—	—	—
	Annual precipitation	1090	0.937	0.8401	0.3297	0.9806	1.69	—	—	—	—	—	—
	Maximum temperature	1090	0.0324	0.0152	0.0272	0.0341	0.0414	—	—	—	—	—	—
	Solar radiation	1090	-0.2172	0.0854	-0.2581	-0.2004	-0.1606	—	—	—	—	—	—
	Nighttime light	1090	0.1507	0.2746	0.000381	0.0392	0.1965	—	—	—	—	—	—
Selected local supplementary mechanism variables (107 only)	Road density	—	—	—	—	—	—	107	1.9381	1.5320	0.8620	1.5969	2.6830
	POI density	—	—	—	—	—	—	107	0.080327	0.487342	0.000000	0.000000	0.000000
	Road length within 2-km buffer	—	—	—	—	—	—	107	24352.9711	19250.4797	10831.0812	20065.6966	33712.7159
	Basic-service POI count	—	—	—	—	—	—	107	1.0093	6.1237	0.0000	0.0000	0.0000
	Basic-service POI density	—	—	—	—	—	—	107	0.0119	0.1156	0.0000	0.0000	0.0000
	Cultural POI density	—	—	—	—	—	—	107	0.000008	0.000049	0.000000	0.000000	0.000000

Note: For the regional background explanatory variables, descriptive statistics are reported for standardized model-input variables rather than for raw physical units. The statistics for the selected local supplementary mechanism variables are reported in their original units.

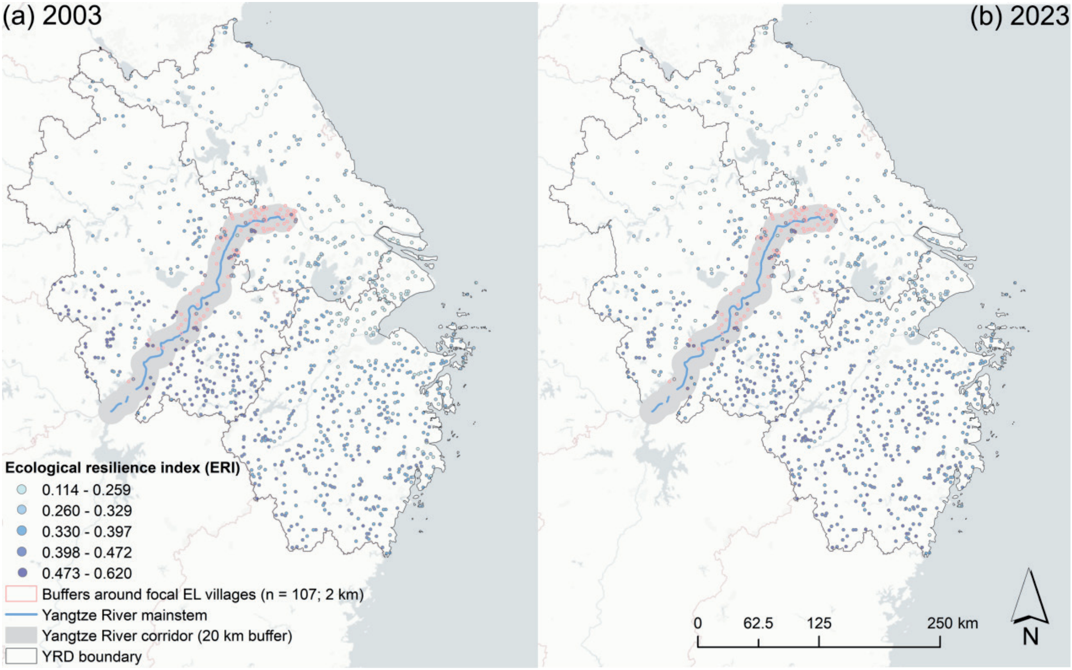

Fig. 3. Spatial distribution of the ecological resilience index (ERI) for the 1,090 ecologically livable villages in the Yangtze River Delta in 2003 and 2023. a) 2003; b) 2023.

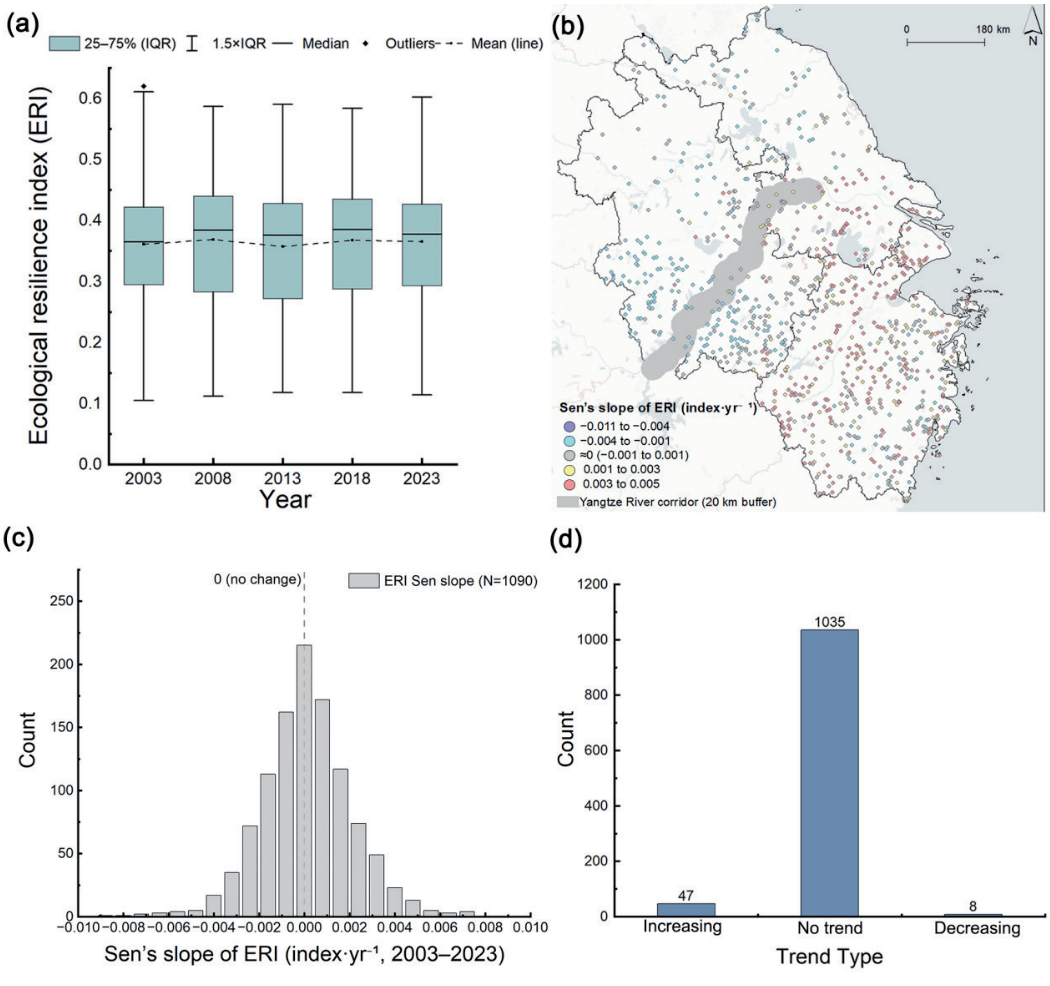

Fig. 4. Temporal distribution and trend characteristics of the ecological resilience index (ERI) in the 1,090 ecologically livable villages in the Yangtze River Delta during 2003-2023. a) Distribution of ERI at five time points; b) spatial distribution of Sen's slope of ERI; c) frequency distribution of Sen's slope of ERI; d) classification of trend types.

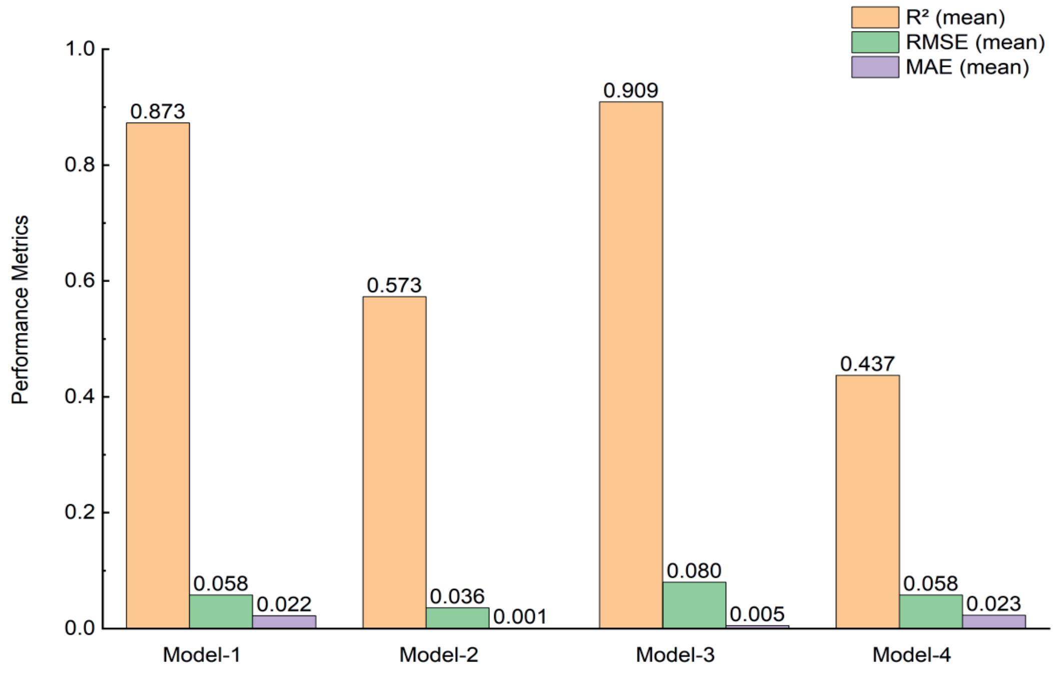

Fig. 5. Predictive performance comparison of the four models. Bars indicate R^2, RMSE, and MAE for each model.

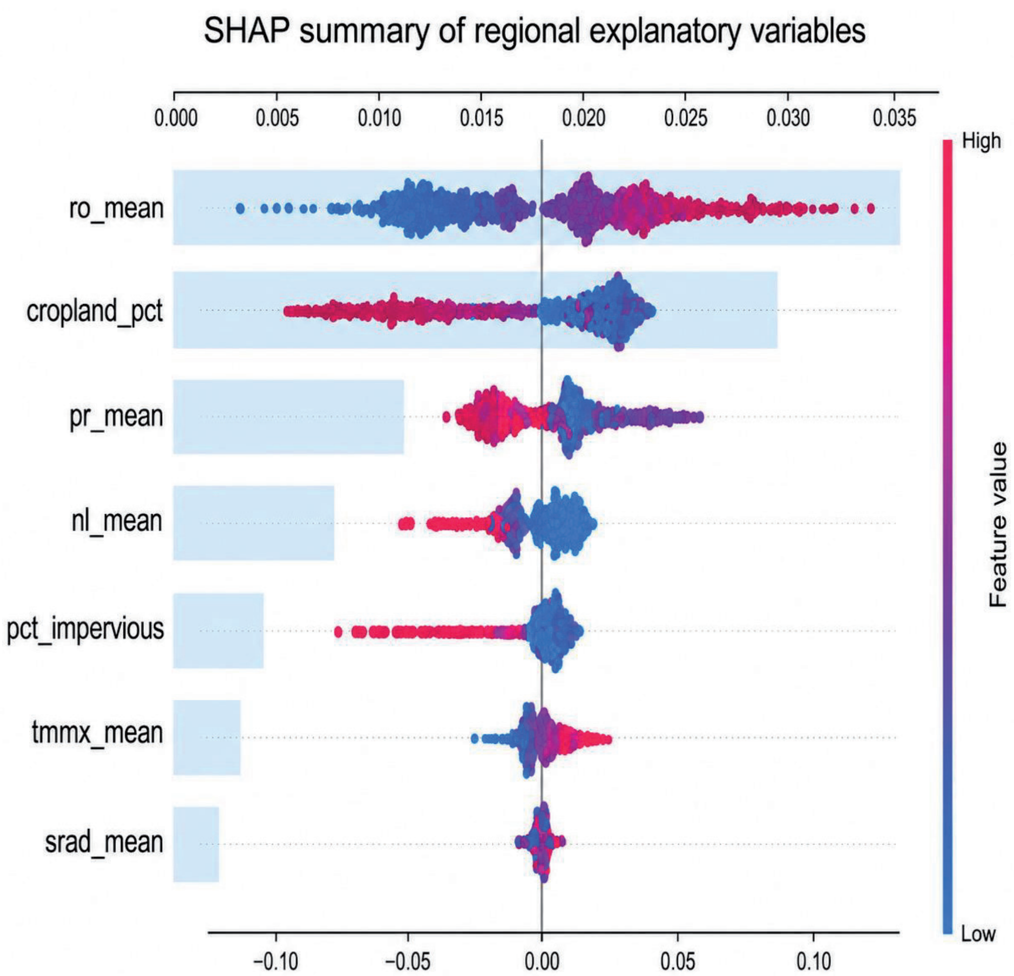

Fig. 6. Combined SHAP summary plot for the key explanatory variables associated with the 2023 ecological resilience index (ERI) in Model-1 (n = 1,090). Bars indicate global feature importance ranked by mean absolute SHAP value, and colored points show the SHAP beeswarm distribution.

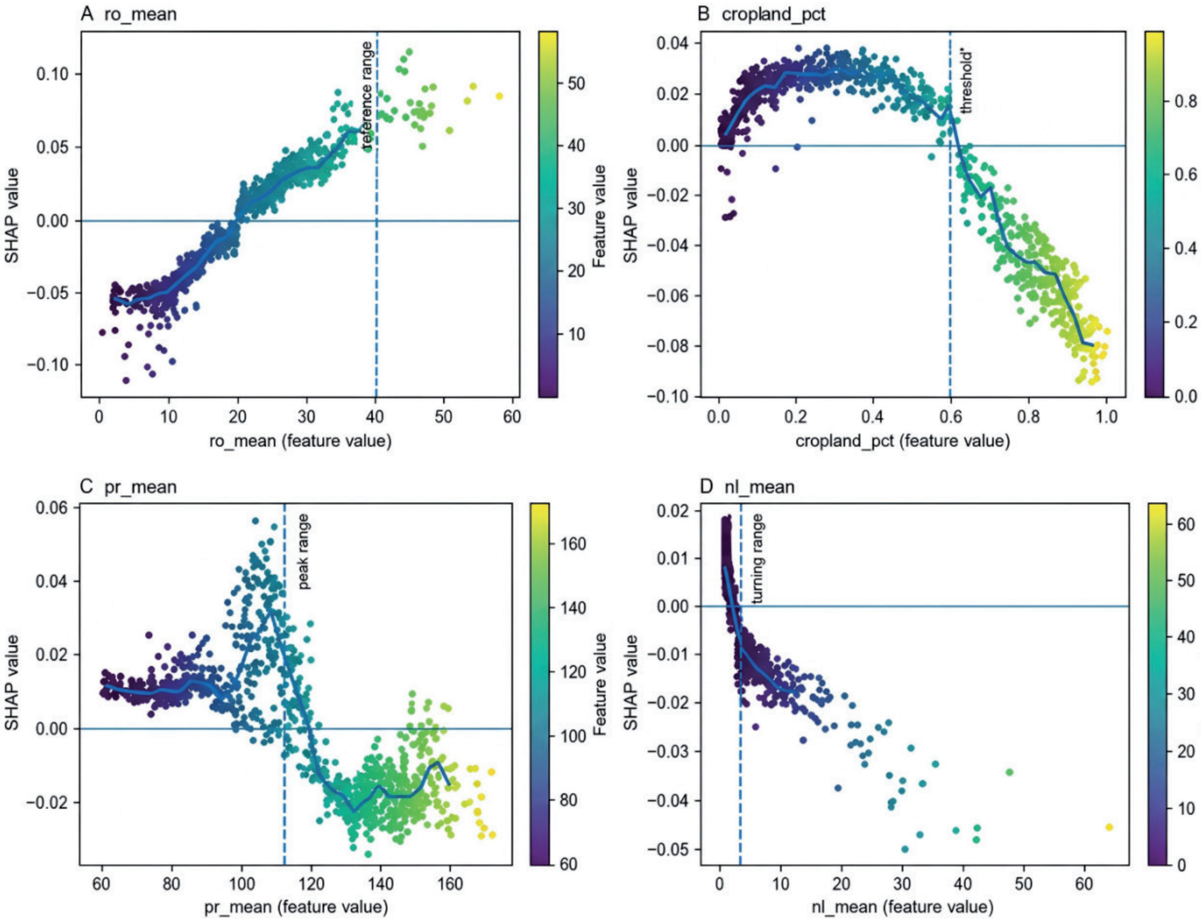

Fig. 7. Nonlinear response characteristics of the key explanatory variables associated with the 2023 ecological resilience index (ERI) in Model-1 (n = 1,090). a) Runoff (ro_mean); b) cropland proportion (cropland_pct); c) precipitation (pr_mean); d) nighttime light (nl_mean). Dashed lines indicate heuristic turning points for visual reference only.

values. cropland_pct showed a more distinct segmented pattern. It was mainly associated with positive SHAP values in the low-to-moderate range, but it declined rapidly after approximately 0.6 and entered the negative range. pr_mean showed a nonlinear pattern of first increasing and then decreasing. It reached a positive peak at approximately 100-110, then declined rapidly, and remained negatively associated with ERI at higher values. nl_mean mainly showed a sharp transition in the low-value range. Its SHAP values were close to zero at very low levels, but dropped quickly into the negative range after the turning point and continued to decrease.

Overall, Fig. 7 shows that the key explanatory variables all had relatively high SHAP contributions, but their SHAP contribution directions and response magnitudes differed markedly across value ranges.

Evidence from Mechanism Variables in the Yangtze Corridor Sample

Fig. 8 presents the results for the mechanism variables in the corridor sample. The global importance ranking shows clear differences in the contributions of the mechanism variables. Road density had the highest mean absolute SHAP value and showed the strongest contribution among the mechanism variables. POI density and road length within the 2-km buffer ranked second and third, respectively. In contrast, basic-service POI count, basic-service POI density, and cultural POI density showed relatively low contributions and remained close to zero overall.

The dependence results further show different local response patterns for road density and road length within the 2-km buffer. Road density was mainly associated with negative SHAP values in the low-value range. Partial positive contributions appeared in the middle range, whereas the SHAP values returned to around zero or became slightly negative again at higher values. By contrast, the dependence pattern of road length within the 2-km buffer was flatter. Most samples were concentrated around zero, and only a small number of observations in the local low-value range showed positive contributions.

Overall, Fig. 8 indicates clear differences among the mechanism variables in their explanatory contributions, SHAP contribution directions, and local distribution ranges in the corridor sample.

Persistent Differentiation under Long-Term Stability

Overall Stability and Persistent Spatial Contrast

Ecological resilience in ecologically livable villages (EL villages) in the Yangtze River Delta changed only slightly during 2003-2023. Most villages had Sen's slope values close to zero, and the vast majority showed no clear trend, indicating a broadly stable regional pattern. However, this overall stability does not mean that internal differences disappeared. Similar findings have been reported in previous studies, where long-term regional stability did not necessarily imply convergence in internal ecological conditions [26, 27].

The southern high-value areas and the Yangtze corridor advantage were evident in both 2003 and 2023, showing that the spatial contrast between higher- and lower-ERI areas persisted over time. This pattern is consistent with previous findings that long-term ecological patterns are often associated with natural background conditions, land-use structure, and regional development contexts [28-30].

Shift from Average Trends to Spatial Heterogeneity

When overall change is limited, the key issue is not the average trend itself but the persistent spatial differences among villages. Previous studies have suggested that, under limited regional average change,

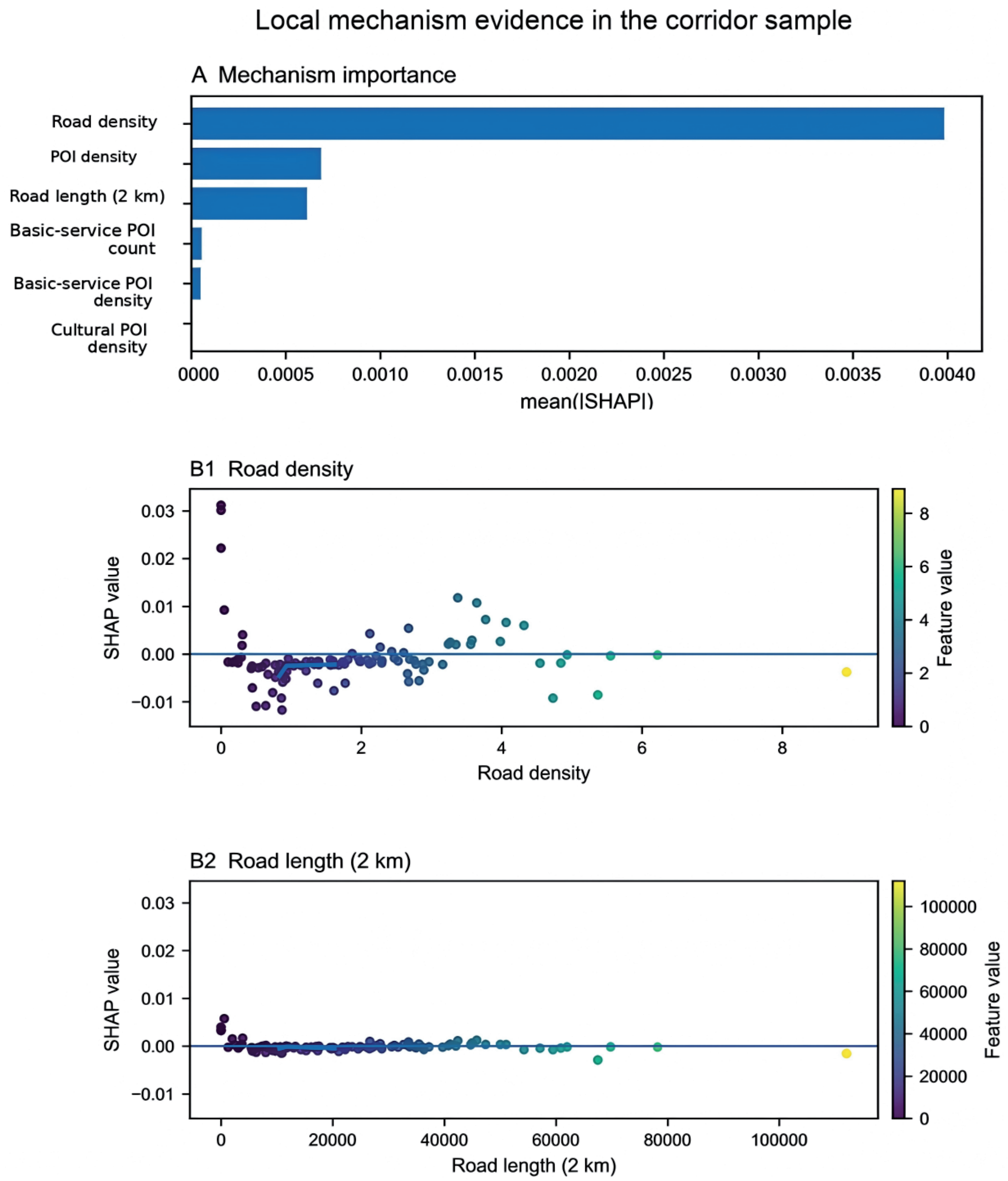

Fig. 8. Local mechanism evidence in the corridor sample. (A) Global importance ranking of mechanism variables by mean absolute SHAP value; (B1) dependence distribution of road density; (B2) dependence distribution of road length within the 2-km buffer. Point colors represent variable values, and the horizontal reference line indicates zero SHAP contribution.

explanatory-variable analysis should shift toward spatial heterogeneity and the conditions under which it is observed [31-33]. Therefore, the following discussion focuses on two levels: regional-scale background explanatory variables and supplementary local mechanism evidence in the Yangtze corridor.

Regional Background Explanatory Variables and Nonlinear Associations

Variable Importance and SHAP Contribution Direction

The regional-scale results show that ERI in 2023 was mainly associated with a small number of high-contribution explanatory variables rather than with many variables of similar importance. Runoff, cropland proportion, and precipitation ranked highest, indicating that hydrological conditions and land-use structure had stronger explanatory power for the current ERI pattern. This finding is consistent with previous studies showing that complex ecological patterns are often more strongly associated with a limited number of key background factors than with the average contribution of all variables [34]. Therefore, variable importance provides a basis for identifying the background conditions associated with regional ERI differences.

Importance ranking alone cannot explain how different variables contributed to ERI predictions. Although runoff, cropland proportion, and precipitation all ranked highly, their SHAP contribution directions differed. High runoff values were clearly associated with positive SHAP contributions, whereas cropland proportion and precipitation showed both positive and negative contributions across samples. This indicates that variable importance should be interpreted together with SHAP contribution direction and response heterogeneity [35, 36].

Sensitive Ranges and Management Relevance

The dependence results further show that the SHAP contributions of the key explanatory variables to ERI did not follow simple monotonic relationships, but varied markedly across value ranges. Runoff showed a gradually increasing positive SHAP contribution pattern. Cropland proportion showed a segmented pattern that shifted from positive to negative. Precipitation showed a nonlinear curve that first increased and then decreased. Nighttime light showed a rapid turning point near the low-value range. These results indicate that the key explanatory variables at the regional scale differed not only in importance, but also in their sensitive ranges.

Compared with linear interpretations, identifying sensitive ranges helps clarify how the same explanatory variable is associated with ERI across different value ranges and provides more targeted evidence for differentiated environmental management [37-39].

Taken together, the regional-scale results show that current ERI differences were associated with long-term environmental background conditions, variable importance, SHAP contribution direction, and sensitive ranges. The corridor analysis therefore further examines whether local environmental and spatial configuration factors can distinguish current differences under similar background conditions.

Supplementary Local Mechanism Evidence from The Yangtze Corridor

Hierarchy of Local Mechanism Variables

The corridor results show a clear hierarchy among local mechanism variables. Road density had the highest mean absolute SHAP value, followed by POI density and road length within the 2-km buffer [40-42]. By contrast, basic-service POI count, basic-service POI density, and cultural POI density showed lower contributions. This does not mean that these variables had no role, but indicates that road accessibility and facility agglomeration had stronger discriminative power for current ERI differences within the Yangtze corridor context [43].

Relationship between Regional and Corridor Analyses

The regional-scale main sample and the corridor sample addressed different explanatory tasks rather than interchangeable analyses. The regional-scale analysis described the natural and climatic background conditions associated with the relatively stable ERI pattern in the Yangtze River Delta [44]. The corridor analysis, by contrast, examined whether local environmental and spatial configuration variables could further distinguish current ERI differences under a similar sensitive-zone context [45].

Therefore, the corridor analysis should be understood as supplementary local mechanism evidence rather than a repetition of the 1,090-village analysis. It extends the regional explanatory-variable analysis to the level of road accessibility, facility agglomeration, and local spatial configuration within the Yangtze corridor.

Environmental Management Implications and Research Boundaries

Environmental Management Implications

The corridor results provide three implications for environmental management and spatial configuration optimization. First, road density, POI density, and road length showed stronger explanatory contributions than other local mechanism variables, suggesting that road accessibility and facility agglomeration should be considered priority factors in corridor villages [46, 47].

Second, importance ranking alone is not sufficient for local intervention. SHAP contribution patterns across value ranges should also be considered, because higher variable values do not always correspond to more positive contributions. Third, regional- and corridor-scale evidence should be used together. Regional-scale results identify background constraints, whereas corridor results help clarify local spatial configuration priorities for differentiated environmental management.

Research Boundaries and Future Research

Although this study links long-term regional-scale evolution, key explanatory-variable identification, and local mechanism evidence under a unified ERI framework, its interpretation has several boundaries. First, the 1,090-village sample and the 107-village corridor sample served different analytical tasks. The former was used to identify long-term regional patterns and natural and climatic explanatory variables, whereas the latter provided supplementary evidence on local mechanisms under the Yangtze corridor context. Therefore, the mechanism findings from the corridor sample should not be directly generalized to all EL villages in the Yangtze River Delta.

Second, the representation of local mechanism variables remains limited. Road, POI, and public-service-related indicators can reflect observable spatial configuration conditions, but they cannot fully represent institutional implementation, organizational coordination, public participation, or local action capacity. Some mechanism variables were also derived from the latest available cross-sectional datasets rather than time-matched observations for 2023. Therefore, the local mechanism results should be interpreted as evidence based on observable spatial conditions rather than as a complete explanation of the governance process [48, 49].

Third, the nonlinear responses and sensitive ranges identified by XGBoost-SHAP should be understood as statistically derived range characteristics rather than fixed thresholds. The SHAP results reflect model-based statistical associations and contribution patterns, not strict causal effects. Thus, the identified sensitive ranges provide interpretive guidance for environmental management, but should not be mechanically applied as universal thresholds.

Fourth, the four models correspond to different analytical tasks, including current ERI levels, long-term trends, and corridor-level mechanism interpretation. Differences in model performance should therefore be understood in relation to these tasks. The lower performance of the trend and change models indicates that long-term ERI evolution is more difficult to explain than current spatial patterns. Future research can expand local mechanism variables to wider areas, introduce more direct process-based indicators, and use longer time series or stronger causal identification strategies to test whether key explanatory variables and sensitive ranges change across time, policy contexts, and regional settings.

Conclusions

Under a unified indicator system, this study developed an analytical framework linking long-term patterns, regional background explanatory variables, and local mechanism analysis in the corridor to explain persistent differentiation within ecologically livable villages (EL villages) in the Yangtze River Delta.

Four main conclusions can be drawn. First, ecological resilience in EL villages in the Yangtze River Delta changed only gradually during 2003-2023, but spatial differences remained throughout the study period. The southern part of the region and villages in the Yangtze corridor generally maintained relatively high resilience levels, whereas most villages did not show a significant long-term increasing or decreasing trend. Second, ERI in 2023 was mainly associated with a small number of key explanatory variables. Runoff, cropland proportion, and precipitation constituted the core explanatory-variable group, followed by nighttime light, whereas the contributions of the other variables were relatively limited. Third, the SHAP contributions of the key explanatory variables did not follow simple linear relationships, but differed clearly across value ranges. This indicates that average associations alone are not sufficient to explain the differentiation of rural ecological resilience. Fourth, the corridor sample provided additional evidence at the local mechanism level. Road density, POI density, and road length showed stronger explanatory contributions, whereas basic-service POI count, basic-service POI density, and cultural POI density had relatively weaker marginal explanatory power. This suggests that, under the corridor context, environmental and spatial configuration conditions can further distinguish current differences in ecological resilience among villages.

The main contribution of this study lies not in ranking individual variables alone. Rather, it lies in linking long-term pattern identification, regional background explanatory-variable analysis, and local mechanism analysis in the corridor under a unified indicator system, thereby providing a multilevel explanation for the persistent differentiation within EL villages. The regional-scale analysis reveals the long-term environmental background constraints underlying the overall pattern, whereas the corridor analysis further supplements the sources of local environmental and spatial configuration differences within this sensitive-zone context. Together, these two parts provide a continuous line of evidence linking the overall pattern to local differences.

Overall, differences among EL villages in the Yangtze River Delta should be understood in relation to both long-term natural and climatic backgrounds at the regional scale and environmental and spatial configuration conditions under local contexts. For environmental management, this means that a single uniform intervention should not be adopted on the basis of average levels alone. Instead, management priorities and spatial configuration differences should be identified under regional background constraints. In particular, for villages in the sensitive zone of the Yangtze corridor, differentiated management should focus on road accessibility, facility agglomeration, and local environmental conditions. This analytical framework provides empirical evidence for environmental assessment, spatial configuration optimization, and differentiated environmental management in EL villages, especially in sensitive corridor zones.

Acknowledgments

The authors would like to thank the supervisor and the related research team for their guidance and support in the research design, data processing, model analysis, and manuscript revision. The authors also gratefully acknowledge the publicly available village lists with an ecological-livability orientation released by national and related institutions, as well as the open databases and data platforms that provided the basic data support for this study.

AI Usage Disclosure Statement

During manuscript preparation, the authors used ChatGPT (OpenAI) only for language polishing and grammar improvement. All scientific analyses, including data processing, ecological resilience assessment, GIS analysis, machine learning modeling, SHAP interpretation, and the conclusions presented in this manuscript, were independently conducted and verified by the authors. The authors take full responsibility for the content and scientific integrity of this work.

Conflict of Interest

The authors declare no conflict of interest.

References

1. GUO Y., LI S. A policy analysis of China's sustainable rural revitalization: integrating environmental, social and economic dimensions. Frontiers in Environmental Science, **12**, 1436869, **2024**.
2. GENG Y., LIU L., CHEN L. Rural revitalization of China: A new framework, measurement and forecast. Socio-Economic Planning Sciences, **89**, 101696, **2023**.
3. WU J., SUN W. Regional integration and sustainable development in the Yangtze River Delta, China: Towards a conceptual framework and research agenda. Land, **12** (2), 470, **2023**.
4. KIM G., KANG W., LEE J. Knowledge structures and components of rural resilience in the 2010s: Conceptual development and implications. Sustainability, **12** (22), 9769, **2020**.
5. WALKER B., HOLLING C.S., CARPENTER S.R., KINZIG A. Resilience, adaptability and transformability in social–ecological systems. Ecology and Society, **9** (2), 5, **2004**.
6. HOLLING C.S. Resilience and stability of ecological systems. Annual Review of Ecology and Systematics, **4**, 1, **1973**.
7. HAN G., WEI Z., ZHENG H., ZHU L. Evaluation index system of rural ecological revitalization in China: A national empirical study based on the driver-pressure-state-impact-response framework. Land, **13** (8), 1270, **2024**.
8. JIA A., YUN X., ZHENG X., WEN X., LIANG X., YUN Y. Towards sustainable rural revitalization: A multidimensional evaluation of rural vitality in China's traditional villages. Sustainability, **16** (13), 5408, **2024**.
9. YANG M., JIAO M., ZHANG J. Spatio-temporal analysis and influencing factors of rural resilience from the perspective of sustainable rural development. International Journal of Environmental Research and Public Health, **19** (19), 12294, **2022**.
10. YANG Y. Research hotspots and evolution trends of rural resilience in the perspective of biodiversity – Based on citeSpace's visual analysis of bibliometrics. Frontiers in Environmental Science, **10**, 1029510, **2022**.
11. LIU R., ZHANG L., TANG Y., JIANG Y. Understanding and evaluating the resilience of rural human settlements with a social-ecological system framework: The case of Chongqing Municipality, China. Land Use Policy, **136**, 106966, **2024**.
12. YING C., LI Y., CHEN Y., ZHONG J., AI S., TIAN P., HUANG Q., CAO L., MOUAZEN A.M. Evolution and prediction of rural ecological environment quality in eastern coastal area of China. Frontiers in Environmental Science, **12**, 1403342, **2024**.
13. NELSON K.S., NGUYEN T.D., FRANCOIS J.R., OJHA S. Rural sustainability methods, drivers, and outcomes: A systematic review. Sustainable Development, **31** (3), 1226, **2023**.
14. LU Y., DE VRIES W.T. A bibliometric and visual analysis of rural development research. Sustainability, **13** (11), 6136, **2021**.
15. ZHU F., YING B., XIANG C. Advancements in rural resilience research over the past two decades and its significance for sustainable development. Discover Sustainability, **6**, 145, **2025**.
16. XU M., ZHAO W., YANG Y., YANG Y., WU J., MUKHTAR H. An improved estimation of remote sensing-based ecological index for tracking continuous changes in eco-environmental quality. International Journal of Digital Earth, **17** (1), 2445625, **2024**.
17. WANG S., LIANG X., WANG J. Parameter assignment for InVEST habitat quality module based on principal component analysis and grey coefficient analysis. Mathematical Biosciences and Engineering, **19** (12), 13928, **2022**.
18. GONG X., LI T., WANG R., HU S., YUAN S. Beyond the remote sensing ecological index: A comprehensive ecological quality evaluation using a Deep-Learning-

Based remote sensing ecological index. Remote Sensing, **17** (3), 558, **2025**.
19. SEN P.K. Estimates of the regression coefficient based on Kendall's tau. Journal of the American Statistical Association, **63** (324), 1379, **1968**.
20. MANN H.B. Nonparametric tests against trend. Econometrica, **13** (3), 245, **1945**.
21. HAMED K.H., RAO A.R. A modified Mann-Kendall trend test for autocorrelated data. Journal of Hydrology, **204** (1-4), 182, **1998**.
22. CHEN T., GUESTRIN C. XGBoost: A scalable tree boosting system. In Proceedings of the 22nd ACM SIGKDD International Conference on Knowledge Discovery and Data Mining, 785, **2016**.
23. LUNDBERG S.M., ERION G., CHEN H., DEGRAVE A., PRUTKIN J.M., NAIR B., KATZ R., HIMMELFARB J., BANSAL N., LEE S.-I. From local explanations to global understanding with explainable AI for trees. Nature Machine Intelligence, **2** (1), 56, **2020**.
24. WANG P., WANG J., LI Y., REN Y., SHI J. Coupling coordination between livelihood resilience and ecological livability for farming households relocated from mining-under villages in eastern China. Land, **14** (6), 1233, **2025**.
25. LI C., LIU Q., ZONG Z., FANG Y. Rural environmental quality evaluation indicator system: application in Shangluo City, Shaanxi Province. Sustainability, **16** (8), 3198, **2024**.
26. TAO T., MA L., LIU Y., TANG H., WANG X., WU S. A systematic framework for rural resilience assessment in the rural Gansu Province, China. Environmental Impact Assessment Review, **110**, 107715, **2025**.
27. WEI Y., WANG W. Rural resilience assessments in the Yangtze River Delta based on the DPSIR model. Sustainability, **17** (10), 4725, **2025**.
28. YIN S., ZHOU Y., ZHANG C., WU N. Impact of regional integration policy on urban ecological resilience: A case study of the Yangtze River Delta region, China. Journal of Cleaner Production, **485**, 144375, **2024**.
29. LE X., DING X., ZHANG J., ZHAO L. Has green finance enhanced the ecological resilience level in the Yangtze River Economic Belt? Sustainability, **16** (7), 2926, **2024**.
30. WANG Z., HUANG W., GUAN X. Ecosystem resilience trends and its influencing factors in China's Three-River Headwater Region: A comprehensive analysis using CSD indicators (1982-2023). Land, **13** (8), 1224, **2024**.
31. LIU J., LI J., WANG Y. Interrelationships and zoning-based management of landscape ecological risk and ecological resilience in the Hefei metropolitan circle from a multi-scale perspective. Frontiers in Environmental Science, **13**, 1654175, **2025**.
32. WU J., ZUO J., LI L., YANG Y., YANG M., LIU S. Evaluation of rural ecological resilience from the perspective of communities and farmers: a study on Laochehe ethnic minority village in China. Environmental Research Communications, **6** (4), 045010, **2024**.
33. CAO W., YANG Q., LIU Y., LIU X., HE H., YANG J., DENG Q., WANG Y. Research on social-ecological resilience assessment of rural settlements in typical mountainous areas of southwest China based on the coordination of kernel and peripheral systems. Land, **14** (10), 2054, **2025**.
34. ZHANG Y., LIU J., ZHU Y. Assessment of ecological resilience and identification of influencing factors in Jilin Province, China. Sustainability, **17** (13), 5994, **2025**.
35. YANG F., YANG L., FANG Q., YAO X. Impact of landscape pattern on habitat quality in the Yangtze River Economic Belt from 2000 to 2030. Ecological Indicators, **166**, 112480, **2024**.
36. YIN S., SHI R., WU N., YANG J. Measuring the impact of technological innovation on urban resilience through explainable machine learning: A case study of the Yangtze River Delta region, China. Sustainable Cities and Society, **127**, 106457, **2025**.
37. WEN C., LONG T., HE G., JIAO W., JIANG W. Temporally enhanced RSEI and nighttime lights reveal long-term ecological changes and effective protection in China's inaugural national parks. Ecological Indicators, **170**, 112981, **2025**.
38. LIANG T., ZHAN J., SU Y., DENG W. Examining the nonlinear effects of multidimensional land use efficiency on ecological resilience using the XGBoost-SHAP and GTWR model in Guangdong province. Frontiers in Environmental Science, **13**, 1697381, **2025**.
39. WU N., ZHOU Y., YIN S., GONG H., ZHANG C. Revealing the nonlinear impact of environmental regulation on ecological resilience using the XGBoost-SHAP model: Evidence from the Yangtze River Delta region, China. Journal of Cleaner Production, **514**, 145700, **2025**.
40. XIAO Y., LIU S., ZUO J., YIN N., WU J., XIE W. Farmer households' livelihood resilience in ethnic tourism villages: A case study of the Wuling mountain area, China. Sustainability, **15** (1), 662, **2023**.
41. ZHANG Y., HUANG J., ZHANG K., GUO Y., HU D., WANG Z. Evaluation of regional characteristics of rural landscapes in the Yangtze River Delta from the perspective of the ecological–production–living concept. Sustainability, **17** (11), 5057, **2025**.
42. NIU J., ZHOU Y. How rural tourism development affects farmers' livelihood resilience: based on comprehensive survey data of rural revitalization in China. Frontiers in Sustainable Food Systems, **9**, 1573149, **2025**.
43. WU J., YANG Y., ZUO J., CAO Q., GUO D., LIU S. Evaluation and influencing factors of ecological resilience in tourism villages from farmers' perspectives: a case study of Chinese minority settlement areas. Frontiers in Environmental Science, **12**, 1400546, **2024**.
44. WANG Y., SONG M., ZHU S., JIANG Z., ZHANG Z. Coupling study on ecological resilience and urban-rural integrated development in China. Frontiers in Environmental Science, **13**, 1552533, **2025**.
45. ZHAO X., CHEN H., ZHAO H., XUE B. Farmer households' livelihood resilience in ecological-function areas: Case of the Yellow River water source area of China. Environment, Development and Sustainability, **24** (7), 9665, **2022**.
46. PENG H., LOU H., LIU Y., HE Q., ZHANG M., YANG Y. Spatial and temporal evolution assessment of landscape ecological resilience based on adaptive cycling in Changsha–Zhuzhou–Xiangtan urban agglomeration, China. Land, **14** (4), 709, **2025**.
47. HUANG J., XUE D., HUANG M. Rural resilience evaluation and risk governance in the middle reaches of the Heihe River, northwest China: An empirical analysis from Ganzhou District, a typical irrigated agricultural area. Land, **14** (5), 926, **2025**.
48. LI E., DENG Q., ZHOU Y. Livelihood resilience and the generative mechanism of rural households out of poverty: An empirical analysis from Lankao County, Henan Province, China. Journal of Rural Studies, **93**, 210, **2022**.

49. LIU M., ZHANG C., LI Z., ABDULAI A., YANG J. Building rural resilience through a neo-endogenous approach in China: Unraveling the metamorphosis of Jianta Village. Agriculture, **15** (21), 2251, **2025**.